THE JOURNAL OF PHYSICAL CHEMISTRY A
A JOURNAL OF THE AMERICAN CHEMICAL SOCIETY

pubs.acs.org/JPCA Article

Ultrafast Decay Dynamics of the $2^1\pi\pi^*$ Electronic State of *N*-Methyl-2-pyridone

Published as part of The Journal of Physical Chemistry A virtual special issue "Xueming Yang Festschrift".

Baihui Feng,[‖] Wenping Wu,[‖] Zhigang He, Dongyuan Yang,* Guorong Wu,* and Xueming Yang

Cite This: *J. Phys. Chem. A* 2024, 128, 3840−3847 Read Online

ACCESS | Metrics & More | Article Recommendations | Supporting Information

ABSTRACT: The ultrafast decay dynamics of *N*-methyl-2-pyridone upon excitation in the near-ultraviolet range of 261.5−227.9 nm is investigated using the femtosecond time-resolved photoelectron spectroscopy method. Irradiation at 261.5 nm prepares *N*-methyl-2-pyridone molecules with high vibrational levels in the $1^1\pi\pi^*$ state. The radiation-less decay to the ground state via internal conversion is suggested to be the dominant channel for the $1^1\pi\pi^*$ state with large vibrational excess energy, which is revealed by a lifetime of 1.6 ± 0.2 ps. As the pump wavelength decreases, we found that irradiation at 238.5 and 227.9 nm results in the population of the $2^1\pi\pi^*$ state. This is in agreement with the assignment of the vapor-phase UV absorption bands of *N*-methyl-2-pyridone. On the basis of the detailed analysis of our measured time-resolved photoelectron spectra at all pump wavelengths, we conclude that the $2^1\pi\pi^*$ state has an ultrashort lifetime of 50 ± 10 fs. In addition, the $S_1(1^1\pi\pi^*)$ state is subsequently populated via internal conversion and decays over a lifetime of 680−620 fs. The most probable whole deactivation pathway of the $2^1\pi\pi^*$ state is discussed. This experimental study provides new insights into the excitation energy-dependent decay dynamics of electronically excited *N*-methyl-2-pyridone.

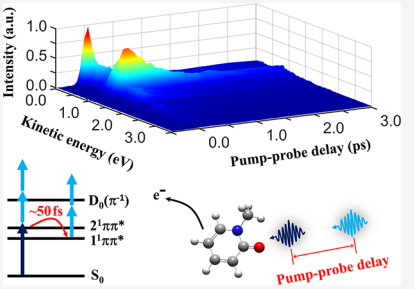

1. INTRODUCTION

Small heterocyclic molecules are key building blocks of biomolecules in nature. For example, three kinds of the five natural DNA/RNA nucleobases, cytosine, thymine, and uracil, are pyrimidine-based organic molecules, the photochemistry of which has been widely studied over the past few decades.[1−6] The excited-state dynamics of prototypical heterocyclic molecules is potentially important for understanding the photoinduced biochemical processes in the earliest stages of prebiotic chemistry.[7,8] In recent years, we have investigated the ultrafast decay dynamics of a series of aromatic heterocyclic molecules containing the nitrogen (N) heteroatom, such as the substituted derivatives of pyrrole[9−13] and pyridine,[14−16] following excitations in the near-ultraviolet (UV) region of their respective electronic absorption spectra. The radiation-less relaxation dynamics of the low-lying electronic excited states of these isolated molecules and the substitution effects on the excited-state dynamics are better understood.

Among these N-containing heterocyclic molecules, 2-pyridone (strictly called 2(*1H*)-pyridone) is one of the simplest six-membered nucleobase analogues, the response of which to UV radiation might be associated with the selection of the important building blocks of life on the early earth.[5] In a recent paper[17] (*J. Phys. Chem. A* **2023**, 127, 10139), we focused solely on a methylated derivative of 2-pyridone, namely, *N*-methyl-2-pyridone (hereafter termed simply NMP), and reported a direct time-resolved study of the ultrafast decay dynamics of NMP excited to the $S_1(1^1\pi\pi^*)$ state. Although there is a keto−enol tautomerization reaction for the parent molecule under our molecular beam conditions,[14,18] methylation of the N position of 2-pyridone removes the possibility of other tautomer and"locks" the pyridone into a keto form. Therefore, in the case of NMP, the excitation energy-dependent decay dynamics can be successfully investigated using the [1 + 1′] femtosecond time-resolved photoelectron spectroscopy (TRPES) method.[17] A clear vibrational-state-dependent lifetime of the S_1 state, which is in the range of several picoseconds to a few nanoseconds, has been revealed by our direct pump−probe measurements. Our gas-phase TRPES study on the isolated NMP molecule has provided valuable and quantitative information about the excited-state lifetime, which can be compared with that in the study of UV-induced dynamics of this molecule in solution.[19] However, the choice of the probe laser wavelength (~239.0 nm) limited the previous time-resolved study when we tuned the pump laser to the deeper UV region close to the probe wavelength. In these cases, the unwanted signals generated from the probe-pump process start to appear in the TRPES spectra. Besides the

Received: March 4, 2024
Revised: April 18, 2024
Accepted: April 18, 2024
Published: May 1, 2024

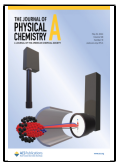

https://doi.org/10.1021/acs.jpca.4c01418
J. Phys. Chem. A 2024, 128, 3840−3847

influence of the probe-pump signals, for pump wavelengths shorter than the probe wavelength of 239.0 nm, the [1 + 1′] TRPES spectra actually have a poor signal-to-noise ratio. As a consequence of these inherent drawbacks, our further attempt to explore the excited-state dynamics of NMP following photoexcitation in the second UV absorption band finally failed. In particular, the decay dynamics of NMP at the pump wavelength of ∼239.0 nm (the probe-pump process) is still less clear-cut and has not been discussed in detail.

In the present work, we continue our efforts and endeavor to investigate the ultrafast decay dynamics of NMP excited to the second optically bright $^1\pi\pi^*$ electronic state. Here, a femtosecond laser pulse of 400.5 nm was chosen as the probe laser for two-photon ionization. Specifically, an ultrashort lifetime of 50 ± 10 fs is obtained and assigned to the $2^1\pi\pi^*$ state at pump wavelengths of 238.5 and 227.9 nm. In addition, evidence of the subsequent population of the $S_1(1^1\pi\pi^*)$ state is experimentally found based on the detailed analysis of the measured [1 + 2′] TRPES spectra. In Section 2, the experimental methods are briefly described. In Section 3, the results derived from the analysis of TRPES spectra are presented, together with further discussions. In Section 4, short conclusions are provided.

2. METHODS

The femtosecond time-resolved photoelectron imaging (fs-TRPEI) experiment was carried out on a velocity map imaging (VMI) spectrometer.[20] Detailed experimental methods have been given in the previous publications of our recent studies on 2-pyridone[18] and NMP.[17] Therefore, only the key features are mentioned here. The liquid NMP sample was purchased from Macklin with a stated purity of ≥98% and was used without further purification. This sample was heated to ∼40 °C throughout the experiment, mixed with 3 bar of helium carrier gas, and expanded supersonically into a high vacuum source chamber via a 1 kHz Even-Lavie valve. The generated molecular beam entered into the interaction chamber of the VMI spectrometer through a 1 mm skimmer located ∼40 mm downstream from the nozzle orifice.

The femtosecond laser system consisted primarily of a fully integrated Ti:sapphire oscillator-regenerative amplifier (Coherent, Libra-HE) and two commercial optical parametric amplifiers (OPA, Coherent, OPerA Solo), each pumped by a fraction (∼1.1 mJ per pulse) of the fundamental 800 nm output of the amplifier. Two different pump wavelengths, 261.5 nm (∼2.0 μJ per pulse) and 238.5 nm (∼0.7 μJ per pulse), were directly obtained from the first OPA. For producing 227.9 nm (∼0.2 μJ per pulse), a 400 nm laser beam, which was the doubling of a fraction of the amplifier fundamental 800 nm output using the first β-barium borate (BaB_2O_4 (BBO)) crystal (0.15 mm), was mixed with the output of the first OPA at ∼529 nm using the second β-BBO crystal (0.1 mm). The probe laser was chosen at 400.5 nm (7−11 μJ per pulse), which was generated by doubling the unused 800 nm output of the second OPA using the third β-BBO crystal (0.1 mm). The bandwidths [full width at half-maximum (fwhm) of the spectrum] of the pump laser pulses were in the range of 214−317 cm^{-1}, and about 334 cm^{-1} for the probe laser pulse of 400.5 nm. The polarization direction of all pump and probe laser pulses was parallel to the microchannel plate (MCP)/phosphor screen detector. The pump and probe laser pulses were combined collinearly on a dichroic mirror without further compression and then focused using a calcium fluoride (CaF_2) lens (f/75 for the pump and f/60 for the probe laser beam) into the interaction region of the VMI spectrometer to intersect the seeded NMP molecular beam. The pump laser pulses excited the supersonic jet-cooled NMP molecules from the ground state to the electronically excited state(s) by one-photon absorption, whereupon the delayed probe laser pulses produced photoelectrons via one-photon and/or two-photon ionization.

The 2D photoelectron images were recorded at different pump−probe time delays by using the computer-controlled camera. The raw images were then transferred to 3D distributions using the pBasex Abel inversion method.[21] The time-dependent photoelectron 3D distributions were further integrated along the recoiling angle to derive the TRPES spectrum. Electron kinetic energy calibration was performed using multiphoton ionization of Xe atoms.[20] The two-color nonresonant ionization of Xe atoms or NO molecules served to measure the time-zero of the experiment. In the meantime, cross-correlation [i.e., instrumental response function (IRF)] between the pump and probe laser pulses was obtained. The [1 + 2′] IRFs were estimated to be 100 ± 15, 130 ± 10, and 115 ± 10 fs (fwhm) for pump wavelengths of 227.9, 238.5, and 261.5 nm respectively, based on the approximation that both pump and probe laser pulses were a Gaussian profile. The fluctuations in the time-zero and uncertainties in the IRF were used to estimate the error bars of the derived time constants during fits of the TRPES data.

3. RESULTS AND DISCUSSION

3.1. UV Absorption Spectrum. The UV absorption spectrum of NMP has been reported in our previous study.[17] Here, it is adapted and is shown in Figure 1. It was measured

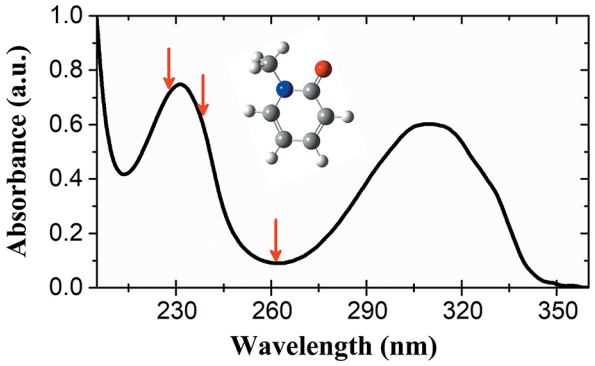

Figure 1. Vapor-phase room-temperature UV absorption spectrum of NMP, a schematic structure of which is the inset. The red arrows indicate the pump wavelengths (261.5, 238.5, and 227.9 nm) used in the current experiment. Adapted with permission from Figure 1 in ref 17. Copyright 2023 American Chemical Society.

under saturated vapor conditions at room temperature using a commercial UV−visible spectrometer (Shimadzu, UV-2700). Briefly, this spectrum consists of three strong absorption bands, with the first and second broad bands being centered at about 310 and 230 nm, respectively. The first absorption band starting from ∼350 nm should be dominated by a $\pi^* \leftarrow \pi$ transition of an electron from the highest occupied molecular orbital (HOMO) to the lowest unoccupied molecular orbital (LUMO) and the $S_1(1^1\pi\pi^*)$ state is mostly excited, while the second band starting from ∼260 nm is mainly ascribed to a mixture of two $\pi^* \leftarrow \pi$ electronic transitions ($\pi^*_{LUMO+1} \leftarrow$

https://doi.org/10.1021/acs.jpca.4c01418
J. Phys. Chem. A 2024, 128, 3840−3847

π_{HOMO} and $\pi^*_{LUMO} \leftarrow \pi_{HOMO-2}$). In addition, the third band starts to be strong for deeper UV wavelengths and should be associated with the higher-lying singlet excited state(s).

3.2. TRPES Spectrum at 261.5 nm. The TRPES spectrum of NMP at a pump wavelength of 261.5 nm is shown in Figure 2a. The [1 + 1′] two-photon energy is insufficient for two-color photoionization of NMP, while the energetic limit for two-color [1 + 2′] ionization to the ground state (D_0) of the NMP cation is calculated using an adiabatic ionization potential of 8.20 eV[22] and indicated by the white dashed line. The main feature of this spectrum is a dominant component that shows a few picoseconds decay dynamics by visual inspection. In order to extract detailed information on time constants and their photoelectron kinetic energy distributions, a 2D global least-squares method was employed to simultaneously fit the TRPES data at all time delays and photoelectron kinetic energies using a well-known Levenberg−Marquardt algorithm. The kinetic model used can be expressed as the following equation:

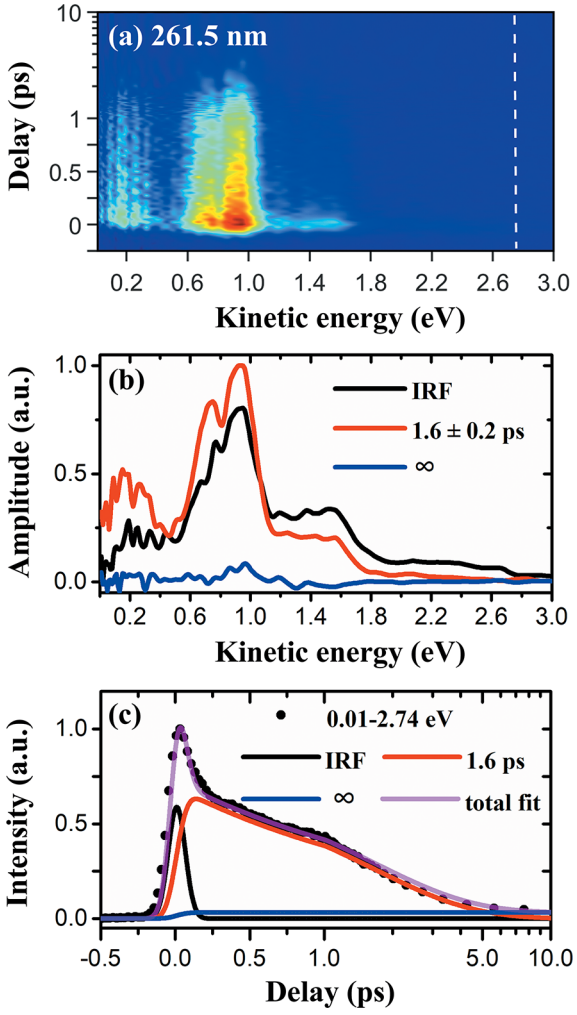

Figure 2. (a) TRPES spectrum of NMP at the pump wavelength of 261.5 nm after subtracting the background photoelectrons generated from single color multiphoton ionization. The energetic limit for two-color [1 + 2′] ionization to the ground state of the NMP cation is indicated by the white dashed line. Note that a combination of linear (≤1 ps) and logarithmic (≥1 ps) scales is used in the ordinate. (b) Photoelectron kinetic energy-dependent amplitudes of each component derived from the 2D global least-squares fit to the TRPES data shown in (a). (c) Normalized photoelectron transient derived by summing the TRPES data shown in (a) over the photoelectron kinetic energy range below the [1 + 2′] energetic limit. The contributions of each component derived from the least-squares fit are also included.

$$S(t, \varepsilon_k) = A_0(\varepsilon_k) \times \mathrm{IRF} + \sum_i A_i(\varepsilon_k) \times \left[\exp\left(-\frac{t}{\tau_i}\right) \times H(t)\right] \otimes \mathrm{IRF} \quad (1)$$

Herein, $S(t, \varepsilon_k)$ represents the 2D TRPES data, while t and ε_k are the time delay and kinetic energy of the emitted photoelectron, respectively. The $A_i(\varepsilon_k)$ represents the photoelectron kinetic energy-resolved amplitudes (also called decay-associated spectra) of the component associated with the time constant, τ_i. $H(t)$ is the Heaviside step function. The corresponding IRF is experimentally measured independently. $A_0(\varepsilon_k) \times$ IRF describes the contribution from the two-color nonresonant photoionization signal and the component associated with a lifetime much smaller than the time resolution of our pump−probe experiment. An overall reasonable and satisfactory fit is achieved for the TRPES data at the pump wavelength of 261.5 nm. The fitting results are presented in Figure 2b. The TRPES data can be integrated over the whole kinetic energy range below the [1 + 2′] energetic limit to derive a photoelectron transient, as shown in Figure 2c. The fit to the experimental data, including the contributions of each component derived from the 2D global least-squares fit, is also presented.

There is a minor contribution associated with the component of ≫1 ns (labeled as ∞ in Figure 2b,c), which shows no decay within the experimental scanning range (a maximum delay of 1 ns was employed in our measurements). This component has very small amplitudes over the whole photoelectron kinetic energy range. This weak signal is most likely to be from the 400.5 nm multiphoton ionization of the metastable intermediates and/or the final products, which are produced by the 261.5 nm pump laser. At a similar pump wavelength, there is no such component of ≫1 ns in the [1 + 1′] TRPES data.[17] Therefore, this component is not associated with the excited-state lifetime and will not be further discussed since it is out of the scope of this work.

The [1 + 2′] TRPES spectrum at a pump wavelength of 261.5 nm (Figure 2a) shows a broad and diffuse distribution over the whole kinetic energy range. Moreover, its main distribution has several peak positions and is far below the corresponding [1 + 2′] energetic limit for ionization to the D_0. Along the time delay coordinate, the TRPES spectrum exhibits fast decay dynamics involving two different time constants, a value of 1.6 ± 0.2 ps and an extremely small one much less than our time resolution (labeled as IRF in Figure 2b,c). Herein, the time constant of 1.6 ± 0.2 ps is assigned to the lifetime of the $S_1(1^1\pi\pi^*)$ state with high vibrational excitation (~1.04 eV above the S_1 origin[23]). For the pump wavelength of 261.5 nm, the value of 1.6 ± 0.2 ps is consistent with the pump wavelength-dependent lifetimes of the S_1 vibrational states derived from the previous [1 + 1′] TRPES data.[17] The component of IRF may include different originations associated with two-color [1 + 2′] three-photon ionization processes around the time-zero.[24] These signals can be approximately described by the corresponding [1 + 2′] IRF.

https://doi.org/10.1021/acs.jpca.4c01418
J. Phys. Chem. A 2024, 128, 3840−3847

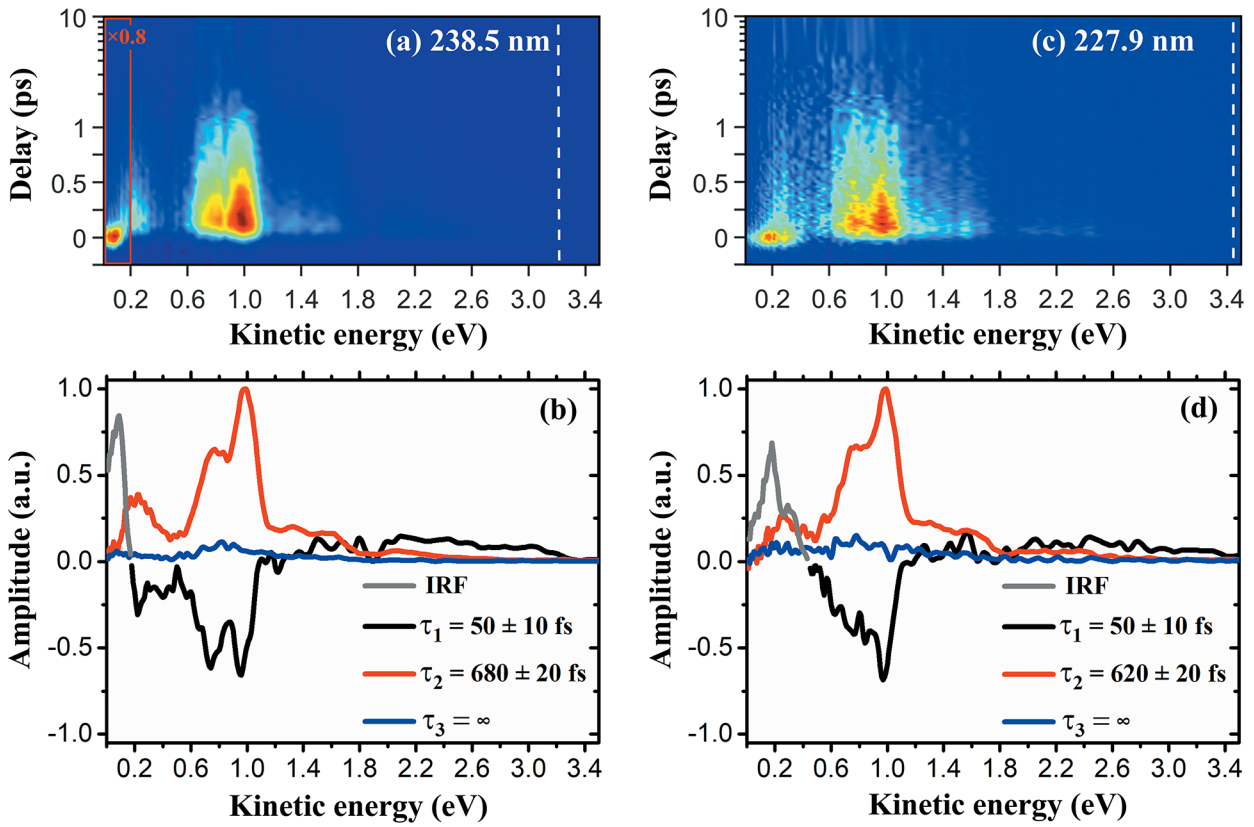

Figure 3. (a) TRPES spectrum of NMP at the pump wavelength of 238.5 nm after subtracting the background photoelectrons generated from single color multiphoton ionization. The energetic limit for two-color [1 + 2′] ionization to the ground state of the NMP cation is indicated by the white dashed line. Note that a combination of linear (≤1 ps) and logarithmic (≥1 ps) scales is used in the ordinate. A portion (<0.20 eV) of the TRPES data is scaled by a factor of 0.8 for better presentation. (b) Photoelectron kinetic energy-dependent amplitudes of each component derived from the 2D global least-squares fit to the TRPES data shown in (a). (c,d) Same as (a,b), but at the pump wavelength of 227.9 nm.

At 261.5 nm, there is no evidence in the [1 + 2′] TRPES spectrum that other electronic excited states higher than the S_1 state start to make a considerable contribution to the photoexcitation.

3.3. TRPES Spectra at 238.5 and 227.9 nm. The TRPES spectrum at the pump wavelength of 238.5 nm is shown in Figure 3a. Note that the [1 + 1′] two-photon energy is sufficient for two-color photoionization of NMP. The expected [1 + 1′] and [1 + 2′] energetic limits for two-color ionization to the D_0 are 0.10 and 3.20 eV, respectively. Therefore, the TRPES spectrum at 238.5 nm could contain both [1 + 1′] and [1 + 2′] two-color photoelectron signals. Such a situation is rare but sometimes can happen.[25] A similar 2D global least-squares method was employed to fit the TRPES data, and three different time constants (labeled as τ_1, τ_2, and τ_3) are needed to achieve an overall satisfactory fit. The decay-associated spectra are presented in Figure 3b. Normalized photoelectron transients derived by integrating the TRPES data over the desired kinetic energy range are shown in Figure 4a−c. The contributions of each component (τ_1, τ_2, and τ_3) are also included. In Figure 4b,c, it is worth mentioning that the contribution (the relative intensity) of τ_1 (50 fs) in the photoelectron transient is much smaller than that of τ_2 (680 fs) due to the different detection efficiency for a given fwhm value of the IRF and a given value of the time constant (τ_i), which can be mathematically described by the result of $\left[\exp\left(-\frac{t}{\tau_i}\right) \times H(t)\right] \otimes$ IRF. A more detailed explanation about this in a similar situation has been given in our recent publication.[16]

As mentioned above in Section 3.2, the component of τ_3 ($\tau_3 = \infty$) will not be further discussed. For the time constant of τ_2, it is straightforward to assign the derived value of 680 ± 20 fs to the lifetime of the highly excited vibrational states of the S_1 state. At high excitation energies, the lifetime of the S_1 vibrational states monotonically decreases with the increase of the vibrational excess energy.[17] Therefore, it is reasonable that the lifetimes of the S_1 state with high vibrational levels are 1.6 ± 0.2 ps at 261.5 nm and 680 ± 20 fs at 238.5 nm. However, the decay-associated spectrum of the τ_1 component has negative amplitudes over the kinetic energy range of about 0.20−1.10 eV, and its overall structure such as the negative peak position is close to that of the decay-associated spectrum of the τ_2 component. This clear evidence strongly indicates that there exists a sequential kinetic process[9,26] (see the Supporting Information for details), which means that the S_1 state is not directly prepared upon excitation at 238.5 nm and is subsequently populated by an ultrafast decay process of internal conversion from a higher-lying excited electronic state to the S_1 state. The component of τ_1 can be approximately described using the time constant with a value of 50 ± 10 fs.

At low kinetic energies around the [1 + 1′] energetic limit for ionization to D_0, the two-color photoelectron signals around time-zero should be primarily from the contribution of the [1 + 1′] nonresonant ionization process. Herein, this signal does not achieve a satisfactory fit when a value of 50 fs is employed for τ_1. In Figure 3b, the time constant of τ_1 is simply

https://doi.org/10.1021/acs.jpca.4c01418
J. Phys. Chem. A 2024, 128, 3840−3847

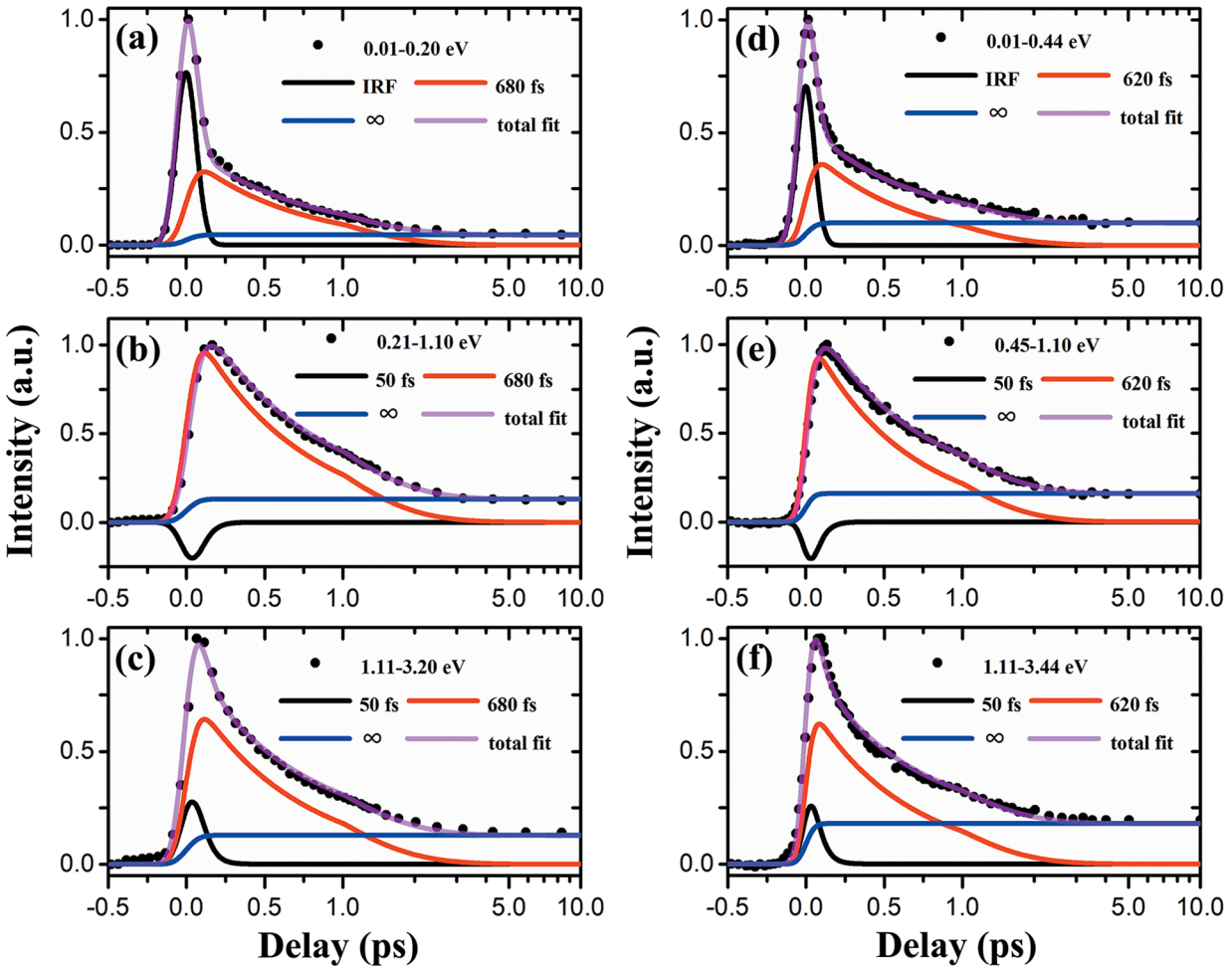

Figure 4. (a–c) Normalized photoelectron transients derived by summing the TRPES data at 238.5 nm over the kinetic energy range of 0.01–0.20, 0.21–1.10, and 1.11–3.20 eV, respectively. The contributions of each component derived from the least-squares fit are also included. (d–f) Same as (a–c), but at 227.9 nm over the kinetic energy range of 0.01–0.44, 0.45–1.10, and 1.11–3.44 eV, respectively.

labeled as IRF at the corresponding low kinetic energies, since $A_0(\varepsilon_k) \times$ IRF can be used instead of the τ_1 component in the fit.

There is one thing that can be clarified here. For the previous [1 + 1′] TRPES study of NMP at a pump/probe wavelength of 258.9/239.0 nm,[17] there was a subpicosecond probe-pump photoelectron signal at very low kinetic energies. This two-color [1 + 1′] signal corresponds to the component of 680 fs in Figure 3b and actually results from ionization of the subsequently populated S_1 vibrational states after the initial relaxation of the $2^1\pi\pi^*$ state based on the analysis described above of the [1 + 2′] TRPES spectrum at 238.5 nm. At pump/probe wavelengths of 339.3–258.9/239.0 nm, the photoelectron signals that were approximately fitted by the IRF and simply ascribed to the two-color [1 + 1′] nonresonant ionization process could be partly associated with the photoexcited decay dynamics of the $2^1\pi\pi^*$ state, the lifetime of which is smaller than the time resolution of the previous [1 + 1′] pump–probe experiments.

For a deeper pump wavelength of 227.9 nm, the TRPES spectrum is shown in Figure 3c. As the pump wavelength decreases, the [1 + 1′] photoelectron signals extend to higher kinetic energies, while the [1 + 2′] signals show little change in the kinetic energy distribution. The corresponding signals are still well below the [1 + 1′] and [1 + 2′] energetic limits for ionization to the D_0 (0.34 and 3.44 eV, respectively). Overall, the TRPES spectrum at 227.9 nm exhibits features identical to those at 238.5 nm. Therefore, a similar way was employed to fit the TRPES data at 227.9 nm and the fitting results are presented in Figures 3d and 4d–f. The assignments of the photoelectron signals are the same as those at 238.5 nm. The $2^1\pi\pi^*$ state with higher vibrational excitation still decays in 50 ± 10 fs, followed by the population of the $S_1(1^1\pi\pi^*)$ state with higher vibrational excess energy, having a lifetime of 620 ± 20 fs.

3.4. Decay Dynamics of the $2^1\pi\pi^*$ State. The ultrafast decay dynamics of the $2^1\pi\pi^*$ state do not show a marked dependence on the pump wavelength. The lifetime of the $2^1\pi\pi^*$ state is measured to be ultrashort, and a value of 50 ± 10 fs is obtained. This suggests that there is a nearly barrierless decay pathway for NMP molecules to evolve from the $2^1\pi\pi^*$ state to lower singlet excited state(s). The high vibrational levels of the $S_1(1^1\pi\pi^*)$ state are subsequently populated within 50 fs, evidenced by the observation of a sequential kinetic process. In Figure 5, the normalized partial photoionization cross sections correlated to the time constant of τ_2 at 228.5 and 227.9 nm are compared with that assigned to the $S_1(1^1\pi\pi^*)$ state at 261.5 nm. Their kinetic energy distributions share large similarities in their overall structure and peak positions. This supports the above assignment of the τ_2 component.

https://doi.org/10.1021/acs.jpca.4c01418
J. Phys. Chem. A 2024, 128, 3840–3847

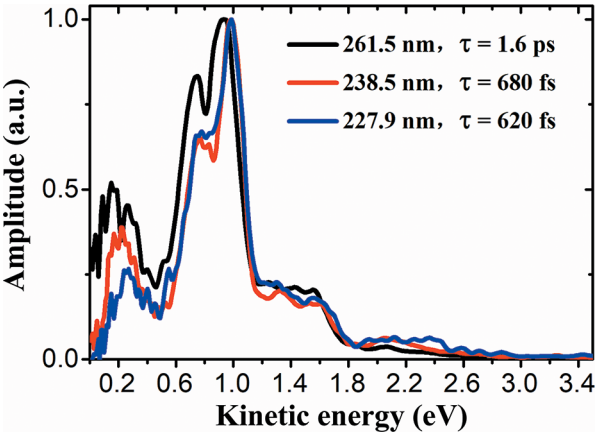

Figure 5. Comparison of the partial photoionization cross sections of the second component in Figures 2b and 3b,d.

Three possible deactivation pathways ($2^1\pi\pi^* \rightarrow 1^1\pi\pi^*$, $2^1\pi\pi^* \rightarrow 2^1n\pi^* \rightarrow 1^1\pi\pi^*$, and $2^1\pi\pi^* \rightarrow 1^1n\pi^* \rightarrow 1^1\pi\pi^*$) can be proposed for photoexcited NMP at 228.5 and 227.9 nm. In the case of the closely related molecule, 2-pyridone, the geometric structures of the singlet electronic excite states ($1^1n\pi^*$, $1^1\pi\pi^*$, $2^1n\pi^*$, and $2^1\pi\pi^*$) and their curve-crossing points were optimized using the CASSCF and CASPT2 methods in a previous study.[27] The short-time structural dynamic of the $2^1\pi\pi^*$ state was revealed and further explained in terms of the existence of a very efficient internal conversion process between the $2^1\pi\pi^*$ state and the $^1n\pi^*$ state. Both the $2^1\pi\pi^*/2^1n\pi^*$ and $2^1\pi\pi^*/1^1n\pi^*$ conical intersections (CIs) were suggested to play a role in the ultrafast internal conversion pathways. Subsequent internal conversion between the $2^1n\pi^*$(or $1^1n\pi^*$) state and the $1^1\pi\pi^*$ state takes place, and the $1^1\pi\pi^*$ state is finally populated. No conical intersection (CI) between the $2^1\pi\pi^*$ state and the $1^1\pi\pi^*$ state was found. Here, in the case of NMP, we infer that the nearby $^1n\pi^*$ dark state(s) may participate in the nonradiative decay of the bright $2^1\pi\pi^*$ excited state. At 238.5 and 227.9 nm, the partial photoionization cross sections of the $2^1\pi\pi^*$ and $1^1\pi\pi^*$ excited states (i.e., the excited state photoelectron spectra), which are shown in Figure 6a,b, are derived from the corresponding decay-associated spectra using the relationship between the decay-associated spectra and the energy-resolved photoionization cross sections in a two-time-constant sequential model[26] (see the Supporting Information for details). Although no signature has been observed of the photoelectron signal of the $^1n\pi^*$ state, it is perhaps due to the overlap of the photoelectron signals ionized from the $2^1\pi\pi^*$, $1^1\pi\pi^*$, $2^1n\pi^*$, and $1^1n\pi^*$ states. Additionally, the lifetime of the $^1n\pi^*$ state should be ultrashort since the $S_1(1^1\pi\pi^*)$ state is populated within 50 fs. Therefore, the partial photoionization cross sections of the initial state (labeled as $2^1\pi\pi^*$ in Figure 6a,b) may include the contribution of the $^1n\pi^*$ state. Thus, it is reasonable to tentatively propose that the intermediate $^1n\pi^*$ ($2^1n\pi^*$ and/or $1^1n\pi^*$) state participates in the decay pathway of the $2^1\pi\pi^*$ state. In other words, the most probable decay pathway can be represented as $2^1\pi\pi^* \rightarrow {}^1n\pi^* \rightarrow 1^1\pi\pi^* \rightarrow S_0$. Direct evidence confirming this assumption remains elusive and may be provided by the femtosecond time-resolved UV-pump-VUV probe [1 + 1′] experiment, which is currently underway in our laboratory. Further theoretical studies are also needed to provide more valuable insights into the UV-photoinduced dynamics of NMP.

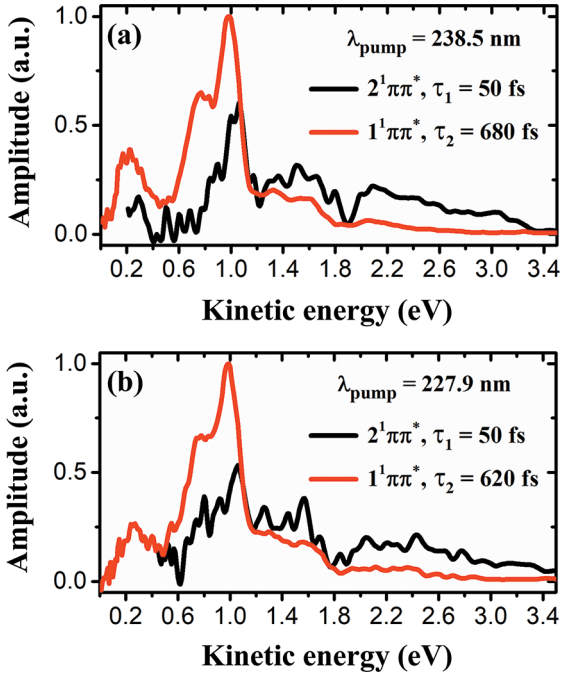

Figure 6. (a) Partial photoionization cross sections derived from the decay-associated spectra at 238.5 nm by assuming a two-step sequential kinetic process. (b) Same as (a) but at 227.9 nm.

4. CONCLUSIONS

In conclusion, the ultrafast decay dynamics of the $2^1\pi\pi^*$ state of NMP following excitations at 238.5 and 227.9 nm is investigated by using the TRPEI technique. The deactivation mechanism of the $2^1\pi\pi^*$ state is proposed based on the detailed analysis of the TRPES spectra. At 238.5 and 227.9 nm, the initially prepared wavepacket on the $2^1\pi\pi^*$ state potential energy surface evolves along appropriate coordinates, and then an ultrafast internal conversion process takes place. It has been shown that the wavepacket funnels down to the $S_1(1^1\pi\pi^*)$ state. This whole radiation-less decay process is within 50 fs. The subsequently populated S_1 state should contain large vibrational excess energy and have a lifetime of 680−620 fs. The decay channel of the S_1 state is most likely to funnel back to the S_0 state via the S_1/S_0 CI.

■ ASSOCIATED CONTENT

Supporting Information

The Supporting Information is available free of charge at https://pubs.acs.org/doi/10.1021/acs.jpca.4c01418.

Sequential kinetic model (PDF)

■ AUTHOR INFORMATION

Corresponding Authors

Dongyuan Yang − *State Key Laboratory of Molecular Reaction Dynamics, Dalian Institute of Chemical Physics, Chinese Academy of Sciences, Dalian, Liaoning 116023, China;* orcid.org/0000-0001-9525-7885; Email: yangdy@dicp.ac.cn

Guorong Wu − *State Key Laboratory of Molecular Reaction Dynamics, Dalian Institute of Chemical Physics, Chinese Academy of Sciences, Dalian, Liaoning 116023, China;*

https://doi.org/10.1021/acs.jpca.4c01418
J. Phys. Chem. A 2024, 128, 3840−3847

orcid.org/0000-0002-0212-183X; Email: wugr@dicp.ac.cn

Authors

Baihui Feng − *State Key Laboratory of Molecular Reaction Dynamics, Dalian Institute of Chemical Physics, Chinese Academy of Sciences, Dalian, Liaoning 116023, China; University of Chinese Academy of Sciences, Beijing 100049, China*

Wenping Wu − *State Key Laboratory of Molecular Reaction Dynamics, Dalian Institute of Chemical Physics, Chinese Academy of Sciences, Dalian, Liaoning 116023, China; University of Chinese Academy of Sciences, Beijing 100049, China*

Zhigang He − *State Key Laboratory of Molecular Reaction Dynamics, Dalian Institute of Chemical Physics, Chinese Academy of Sciences, Dalian, Liaoning 116023, China*

Xueming Yang − *State Key Laboratory of Molecular Reaction Dynamics, Dalian Institute of Chemical Physics, Chinese Academy of Sciences, Dalian, Liaoning 116023, China; Department of Chemistry, College of Science, Southern University of Science and Technology, Shenzhen 518055, China;* orcid.org/0000-0001-6684-9187

Complete contact information is available at: https://pubs.acs.org/10.1021/acs.jpca.4c01418

Author Contributions

[‖]B.F. and W.W. contributed equally to this work.

Notes

The authors declare no competing financial interest.

■ ACKNOWLEDGMENTS

This work was financially supported by the National Natural Science Foundation of China (grant nos. 22203095, 22103087, 22288201, and 21833003), the Key Technology Team of the Chinese Academy of Sciences (grant no. GJJSTD20220001), and the State Key Laboratory of Molecular Reaction Dynamics (grant no. SKLMRD-Z202406). The authors also gratefully acknowledge the support and assistance provided by the Dalian Coherent Light Source (DCLS).

■ REFERENCES

(1) Crespo-Hernández, C. E.; Cohen, B.; Hare, P. M.; Kohler, B. Ultrafast Excited-State Dynamics in Nucleic Acids. *Chem. Rev.* **2004**, *104*, 1977−2019.

(2) Ullrich, S.; Schultz, T.; Zgierski, M. Z.; Stolow, A. Electronic Relaxation Dynamics in DNA and RNA Bases Studied by Time-Resolved Photoelectron Spectroscopy. *Phys. Chem. Chem. Phys.* **2004**, *6*, 2796−2801.

(3) Canuel, C.; Mons, M.; Piuzzi, F.; Tardivel, B.; Dimicoli, I.; Elhanine, M. Excited States Dynamics of DNA and RNA Bases: Characterization of a Stepwise Deactivation Pathway in the Gas Phase. *J. Chem. Phys.* **2005**, *122*, No. 074316.

(4) Marchetti, B.; Karsili, T. N. V.; Ashfold, M. N. R.; Domcke, W. A 'Bottom up', Ab Initio Computational Approach to Understanding Fundamental Photophysical Processes in Nitrogen Containing Heterocycles, DNA Bases and Base Pairs. *Phys. Chem. Chem. Phys.* **2016**, *18*, 20007−20027.

(5) Boldissar, S.; de Vries, M. S. How Nature Covers Its Bases. *Phys. Chem. Chem. Phys.* **2018**, *20*, 9701−9716.

(6) Mu, X.; Zhang, M.; Feng, J.; Yang, H.; Medvedev, N.; Liu, X.; Yang, L.; Wu, Z.; Xu, H.; Li, Z. Identification of the Decay Pathway of Photoexcited Nucleobases. *Ultrafast Sci.* **2023**, *3*, No. 0015.

(7) Lazcano, A.; Miller, S. L. The Origin and Early Evolution of Life: Prebiotic Chemistry, the Pre-Rna World, and Time. *Cell* **1996**, *85*, 793−798.

(8) Powner, M. W.; Gerland, B.; Sutherland, J. D. Synthesis of Activated Pyrimidine Ribonucleotides in Prebiotically Plausible Conditions. *Nature* **2009**, *459*, 239−242.

(9) Wu, G.; Neville, S. P.; Schalk, O.; Sekikawa, T.; Ashfold, M. N. R.; Worth, G. A.; Stolow, A. Excited State Non-Adiabatic Dynamics of N-Methylpyrrole: A Time-Resolved Photoelectron Spectroscopy and Quantum Dynamics Study. *J. Chem. Phys.* **2016**, *144*, No. 014309.

(10) Yang, D.; Chen, Z.; He, Z.; Wang, H.; Min, Y.; Yuan, K.; Dai, D.; Wu, G.; Yang, X. Ultrafast Excited-State Dynamics of 2,4-Dimethylpyrrole. *Phys. Chem. Chem. Phys.* **2017**, *19*, 29146−29152.

(11) Yang, D.; Min, Y.; Chen, Z.; He, Z.; Yuan, K.; Dai, D.; Yang, X.; Wu, G. Ultrafast Excited-State Dynamics of 2,5-Dimethylpyrrole. *Phys. Chem. Chem. Phys.* **2018**, *20*, 15015−15021.

(12) Yuan, W.; Yang, D.; Feng, B.; Min, Y.; Chen, Z.; Yu, S.; Wu, G.; Yang, X. Ultrafast Decay Dynamics of Electronically Excited 2-Ethylpyrrole. *Phys. Chem. Chem. Phys.* **2021**, *23*, 17625−17633.

(13) Yuan, W.; Feng, B.; Yang, D.; Min, Y.; Yu, S.; Wu, G.; Yang, X. Ultrafast Decay Dynamics of N-Ethylpyrrole Excited to the S_1 Electronic State: A Femtosecond Time-Resolved Photoelectron Imaging Study. *Chin. J. Chem. Phys.* **2021**, *34*, 386−392.

(14) Min, Y.; Yuan, W.; Yang, D.; Dai, D.; Yu, S.; Wu, G.; Yang, X. Ultrafast Decay Dynamics of 2-Hydroxypyridine Excited to S_1 Electronic State. *Chin. J. Chem. Phys.* **2022**, *35*, 242−248.

(15) Feng, B.; Yang, D.; Min, Y.; Gao, Q.; Fang, B.; Wu, G.; Yang, X. Excitation Wavelength Dependent S_1-State Decay Dynamics of 2-Aminopyridine and 3-Aminopyridine. *Phys. Chem. Chem. Phys.* **2023**, *25*, 17403−17409.

(16) Feng, B.; Wu, W.; Yang, S.; He, Z.; Fang, B.; Yang, D.; Wu, G.; Yang, X. Insights into Ultrafast Decay Dynamics of Electronically Excited Pyridine-N-Oxide. *Phys. Chem. Chem. Phys.* **2024**, *26*, 8308−8317.

(17) Feng, B.; Yang, D.; He, Z.; Fang, B.; Wu, G.; Yang, X. Excitation Energy-Dependent Decay Dynamics of the S_1 State of N-Methyl-2-Pyridone. *J. Phys. Chem. A* **2023**, *127*, 10139−10146.

(18) Yang, D.; Min, Y.; Feng, B.; Yang, X.; Wu, G. Vibrational-State Dependent Decay Dynamics of 2-Pyridone Excited to the S_1 Electronic State. *Phys. Chem. Chem. Phys.* **2022**, *24*, 22710−22715.

(19) Murdock, D.; Harris, S. J.; Clark, I. P.; Greetham, G. M.; Towrie, M.; Orr-Ewing, A. J.; Ashfold, M. N. R. Uv-Induced Isomerization Dynamics of N-Methyl-2-Pyridone in Solution. *J. Phys. Chem. A* **2015**, *119*, 88−94.

(20) He, Z.; Chen, Z.; Yang, D.; Dai, D.; Wu, G.; Yang, X. A New kHz Velocity Map Ion/Electron Imaging Spectrometer for Femtosecond Time-Resolved Molecular Reaction Dynamics Studies. *Chin. J. Chem. Phys.* **2017**, *30*, 247−252.

(21) Garcia, G. A.; Nahon, L.; Powis, I. Two-Dimensional Charged Particle Image Inversion Using a Polar Basis Function Expansion. *Rev. Sci. Instrum.* **2004**, *75*, 4989−4996.

(22) Cook, M. J.; El-Abbady, S.; Katritzky, A. R.; Guimon, C.; Pfister-Guillouzo, G. Photoelectron Spectra of Hydroxy- and Mercapto-Pyridines and Models of Fixed Structure. *J. Chem. Soc., Perkin Trans.* **1977**, *2*, 1652−1656.

(23) Pradhan, B.; Singh, B. P.; Nandi, C. K.; Chakraborty, T.; Kundu, T. Origin of Methyl Torsional Barrier in 1-Methyl-2-(1H)-Pyridone. *J. Chem. Phys.* **2005**, *122*, 204323.

(24) Yang, D.; Min, Y.; Chen, Z.; He, Z.; Chen, Z.; Yuan, K.; Dai, D.; Wu, G.; Yang, X. Ultrafast Dynamics of Water Molecules Excited to Electronic F∼ States: A Time-Resolved Photoelectron Spectroscopy Study. *Chin. J. Chem. Phys.* **2019**, *32*, 53−58.

(25) Geng, T.; Ehrmaier, J.; Schalk, O.; Richings, G. W.; Hansson, T.; Worth, G.; Thomas, R. D. Time-Resolved Photoelectron Spectroscopy Studies of Isoxazole and Oxazole. *J. Phys. Chem. A* **2020**, *124*, 3984−3992.

(26) Wu, G.; Boguslavskiy, A. E.; Schalk, O.; Schuurman, M. S.; Stolow, A. Ultrafast Non-Adiabatic Dynamics of Methyl Substituted Ethylenes: The π3s Rydberg State. *J. Chem. Phys.* **2011**, *135*, 164309.

(27) Zhang, T.; Xue, J.; Zheng, X.; Xie, B.; Fang, W. Short-Time Dynamics and Decay Mechanism of 2(1H)-Pyridinone Upon Excitation to the Light-Absorbing $S_4(2^1\pi\pi^*)$ State. *J. Chem. Phys.* **2017**, *146*, 114305.

https://doi.org/10.1021/acs.jpca.4c01418
J. Phys. Chem. A 2024, 128, 3840−3847